communications materials

Article

https://doi.org/10.1038/s43246-024-00456-w

Nodal superconductivity in miassite $Rh_{17}S_{15}$

Hyunsoo Kim[1,2,6], Makariy A. Tanatar[1,2], Marcin Kończykowski[3], Romain Grasset[3], Udhara S. Kaluarachchi[1,2], Serafim Teknowijoyo[1,2], Kyuil Cho[1,7], Aashish Sapkota[1], John M. Wilde[1,2], Matthew J. Krogstad[4], Sergey L. Bud'ko[1,2], Philip M. R. Brydon[5], Paul C. Canfield[1,2] & Ruslan Prozorov[1,2] ✉

Solid state chemistry has produced a plethora of materials with properties not found in nature. For example, high-temperature superconductivity in cuprates is drastically different from the superconductivity of naturally occurring metals and alloys and is frequently referred to as unconventional. Unconventional superconductivity is also found in other synthetic compounds, such as iron-based and heavy-fermion superconductors. Here, we report compelling evidence of unconventional nodal superconductivity in synthetic samples of $Rh_{17}S_{15}$ (T_c = 5.4 K), which is also found in nature as the mineral miassite. We investigated the temperature-dependent variation of the London penetration depth $\Delta\lambda(T)$ and the disorder evolution of the critical superconducting temperature T_c and the upper critical field $H_{c2}(T)$ in single crystalline $Rh_{17}S_{15}$. We found a $T-$ linear temperature variation of $\Delta\lambda(T)$ below $0.3T_c$, which is consistent with the presence of nodal lines in the superconducting gap of $Rh_{17}S_{15}$. The nodal character of the superconducting state is supported by the observed suppression of T_c and $H_{c2}(T)$ in samples with a controlled level of non-magnetic disorder introduced by 2.5 MeV electron irradiation. We propose a nodal sign-changing superconducting gap in the A_{1g} irreducible representation, which preserves the cubic symmetry of the crystal and is in excellent agreement with the derived superfluid density. To the best of our knowledge, this establishes miassite as the only mineral known so far that reveals unconventional superconductivity in its clean synthetic form, though it is unlikely that it is present in natural crystals because of unavoidable impurities that quickly destroy nodal superconductivity.

Materials that can display superconductivity are extremely rare in nature. Although some elements are found in metallic form, superconductivity has only been reported in meteorites that contain alloys of tin, lead, and indium[1]. Superconducting compounds are even scarcer, and only the mineral covellite, CuS, shows superconductivity in samples that occur naturally[2], a discovery that occurred many decades after superconductivity was first detected in laboratory-grown CuS crystals[3]. We know of only three other minerals where synthetic analogs are superconductors: parkerite, $Ni_3Bi_2S_2$, with superconducting transition temperature, $T_c \approx 0.7$ K[4,5], and two isostructural compounds, miassite, $Rh_{17}S_{15}$ (T_c = 5.8 K)[6], and palladseite, $Pd_{17}Se_{15}$ (T_c = 2.2 K)[7]. Here, we study the superconducting properties of synthetic miassite, which is also one of the few rhodium-containing minerals. Initially believed to have Rh_9S_8 composition, this compound was first synthesized in the 1930s[8], and superconductivity in polycrystals was reported in 1954 by Matthias et al.[6]. Stoichiometry was refined to $Rh_{17}S_{15}$ in the early 1960s[9]. A mineral with the same composition was discovered significantly later in the placers of the Miass River in the Ural Mountains in Russia, from which it derives its name[10,11]. Natural miassite is found in iso-ferroplatinum deposits as small rounded inclusions up to 100 μm in

[1]Ames National Laboratory, Iowa State University, Ames, IA 50011, USA. [2]Department of Physics & Astronomy, Iowa State University, Ames, IA 50011, USA. [3]Laboratoire des Solides Irradiés, CEA/DRF/IRAMIS, École Polytechnique, CNRS, Institut Polytechnique de Paris, F-91128 Palaiseau, France. [4]Materials Science Division, Argonne National Laboratory, Lemont, IL 60439, USA. [5]Department of Physics and MacDiarmid Institute for Advanced Materials and Nanotechnology, University of Otago, P.O. Box 56, Dunedin 9054, New Zealand. [6]Present address: Department of Physics, Missouri University of Science and Technology, Rolla, MO 65409, USA[7]Present address: Department of Physics, Hope College, Holland, MI 49423, USA. ✉e-mail: prozorov@ameslab.gov

diameter[12]. The natural mineral contains a large amount of impurities, such as iron, nickel, platinum, and copper, at a level of a few atomic percent[13].

The superconducting properties of miassite display a number of remarkable features. It is exceptional among the naturally occurring superconductors, showing an anomalously high upper critical field greater than 20 T[14], exceeding the Pauli limit of about 10 T. In contrast, the upper critical field of palladseite is about 3.3 T, below the Pauli limit[7], while in elemental superconductors, covellite[2,15] and parkerite[4] the upper critical field is orders of magnitude smaller. The heat capacity jump at T_c is reported to significantly exceed the prediction of the weak-coupling Bardeen–Cooper–Schrieffer (BCS) theory[11]. The electronic heat capacity in the normal state shows a large Sommerfeld coefficient[11,16], comparable to heavy-fermion superconductors[17] and probably originates from Rh *d*-electrons[18]. The low-temperature variation of the heat capacity measured in single crystals deviates from the exponential attenuation expected in a fully gapped superconductor[7], contradicting previous findings in polycrystalline samples[16]. The Hebel–Schlichter peak is notably absent in $Rh_{17}S_{15}$, contrary to expectations for *s*-wave superconductivity[16]. We note that the experimental results in the isostructural palladseite are much more consistent with the BCS *s*-wave theory[7]. Finally, there is an order of magnitude difference between the coherence length of about 4 nm derived from $H_{c2}(0)$, and the BCS length scale $\xi_0 \approx 39$ nm, which is at least ten times greater. In the weak-coupling BCS theory, in the clean limit (which we prove is the case here), these two lengths are of the same order, $\xi = 0.87\xi_0$ for isotropic *s*-wave[19] and similarly, with a slightly different numerical prefactor, for arbitrary *k*-dependent order parameter, including *d*-wave[20]. Therefore, an extremely high $H_{c2}(0)$ alone represents a significant departure from the BCS theory.

The unusual experimental observations in $Rh_{17}S_{15}$ motivated us to clarify its superconducting pairing state. In this report, we present strong evidence for an unconventional gap structure in $Rh_{17}S_{15}$. Our discovery is based on measurements of the temperature-dependent London penetration depth, down to $\sim T_c/100$, and the response to non-magnetic disorder. London penetration depth shows *T*-linear variation below $T_c/3$, consistent with the line nodes in the superconducting order parameter[21,22]. Further evidence of a nodal gap is provided by the significant suppression of T_c and H_{c2} by non-magnetic defects induced by 2.5 MeV electron irradiation. Our results are consistent with an extended *s*-wave state that has circular line nodes. The existence of gap nodes is a hallmark of unconventional superconductivity, observed in cuprates[21,23], some iron pnictides[24–27], heavy-fermions[17], and possibly organic superconductors[28]. All of these materials are products of synthetic solid-state chemistry and are not found in nature. Our work establishes $Rh_{17}S_{15}$ as a unique member of the unconventional superconductors, being the only example that occurs as a natural mineral.

Results

London penetration depth

London penetration depth measurements were carried out using the tunnel diode resonator (TDR) technique[29] in a dilution refrigerator to access temperatures significantly below T_c, as low as $\sim T_c/100$[30] (see Supplementary Note 1 for details). Figure 1a shows the variation of London penetration depth, $\Delta\lambda(T)$, in an as-grown single crystal (S-1) measured in both a ^{3}He cryostat (black full symbols) and a dilution refrigerator[30] (blue open symbols), showing almost perfect agreement between the two measurements. As shown in the inset, the pristine sample exhibits a sharp superconducting transition at $T_c = 5.31$ K, determined by the temperature of a maximum of $d\Delta\lambda(T)/dT$. It is sufficiently close to the temperature of zero resistance and is consistent with that determined by heat capacity and magnetization measurements. A photograph of an as-grown single crystal is also shown in the inset in Fig. 1a. The main panel of Fig. 1a presents the behavior of $\Delta\lambda(T)$ below $0.3T_c$, where it shows a linear dependence on the temperature, $\Delta\lambda(T) \propto T$. In this temperature range, the magnitude of the superconducting gap is nearly constant, and the temperature dependence of the penetration depth reflects the gap anisotropy[22]. Our results are inconsistent with a full superconducting gap in $Rh_{17}S_{15}$, which would imply an exponential

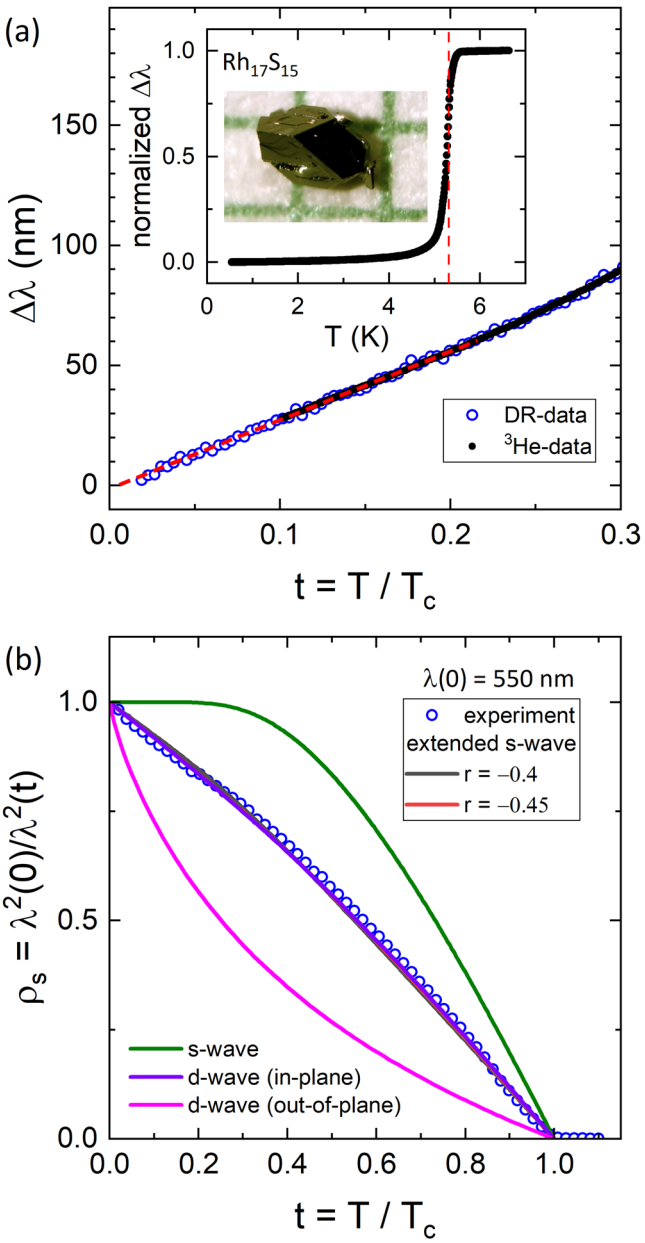

Fig. 1 | London penetration depth and superfluid density in $Rh_{17}S_{15}$. a The temperature variation of London penetration depth, $\Delta\lambda(T)$, in an as-grown single crystal $Rh_{17}S_{15}$. The main panel shows a *T*-linear variation of $\Delta\lambda(T)$ in a characteristic temperature range below $0.3T_c$. The open and closed symbols represent data taken by TDR setups in the dilution refrigerator (DR-TDR) and ^{3}He system (^{3}He-TDR), respectively. Inset: the full temperature range graph of $\Delta\lambda(T)/\Delta\lambda(6\,\mathrm{K})$ and the photograph of a typical single crystal on a 1 mm-scale paper. The dashed vertical line indicates T_c determined by using $d\lambda/dT$ maximum criterion. **b** Normalized superfluid density $\rho_s = \lambda^2(0)/\lambda^2(T)$ in $Rh_{17}S_{15}$. The lines represent the theoretical curves for the full-gap *s*-wave (green), the line-nodal *d*-wave in-plane (violet) and out-of-plane (magenta), and the anisotropic *s*-wave (gray and red) pairing types. A parameter *r* is defined in Eq. (1). Note that the curves for *d*-wave and extended *s*-wave are nearly identical and cannot be distinguished on the figure.

saturation of the penetration depth at low temperatures[22,31]. Instead, the *T*-linear variation of $\Delta\lambda(T)$ in $Rh_{17}S_{15}$ is characteristic of superconductors with line nodes in the clean limit, similar to the experimental observations in the high $-T_c$ cuprates[21]. Notably, in our experiments, this *T*-linear behavior extends down to very low temperatures, $\sim T_c/100$, placing a strenuous upper limit on possible deep gap minima.

The near-perfect *T*-linear behavior observed in our experiments implies that our samples are in the clean limit. Indeed, the very short

coherence length $\xi(0) \approx 4$ nm, due to a very large $H_{c2}(0) \approx 20$ T, is smaller than the mean free path, which can be estimated using Hall effect measurements of carrier mobilities and concentrations at T_c[32], which yields $\ell \approx 86$ nm for $\rho(T_c) \approx 10\,\mu\Omega$cm supporting the clean limit of our $Rh_{17}S_{15}$ crystals.

Superfluid density and superconducting energy gap

The superconducting gap structure can be analyzed using the temperature-dependent normalized superfluid density, $\rho_s(T) = \lambda^2(0)/\lambda^2(T)$. The absolute value of λ at $T = 0$ cannot be directly determined from our measurements of $\Delta\lambda(T)$. The reported values of $\lambda(0)$ in the literature vary from 490 nm determined from $H_{c1}(0) = 30$ Oe[14] to 750 nm from μSR studies[33]. Taking into account such a significant uncertainty in $\lambda(0)$, we used the thermodynamic Rutgers relation, $[d\rho_s(t=1)/dt]/\lambda^2(0) = 16\pi^2 T_c \Delta C/\phi_0[dH_{c2}(t=1)/dt]$, where $t = T/T_c$, $\phi_0 = 2.07 \times 10^{-7}$ G cm^2 is a magnetic flux quantum[34], and heat capacity jump at T_c, ΔC, was taken from Uhlarz et al.[35], see Supplementary Note 2 for details. We obtain $\lambda(0) = 550$ nm, which is between the two values in the literature. As can be seen in Fig. 1b, the normalized superfluid density, ρ_s, of $Rh_{17}S_{15}$ is very different from the expectations of full-gap s-wave superconductors (green line). The choice of $\lambda(0)$ does not qualitatively alter the overall temperature dependence, which is the main criterion to probe the gap anisotropy; see the supporting material. We do not observe any characteristic features of a multigap superconducting state, such as the concave curvature of $\rho_s(T)$ at elevated temperatures. Although $Rh_{17}S_{15}$ is a multiband material, as shown by band structure calculations[36] and Hall effect measurements[32], its superconducting state is characterized by a single gap, consistent with conclusions from heat capacity measurements[16]. Similar behavior is observed in other materials, for example, $SrPd_2Ge_2$, in which a sign-changing Hall effect suggests multi-band transport in the normal state[37], but the superconductivity is still characterized by a single isotropic gap[38].

The penetration depth measurements clearly indicate that a gap with line nodes is realized in $Rh_{17}S_{15}$. Since Knight shift experiments indicate a spin-singlet order parameter[16], the orbital component of the pair potential must be even parity. A possible gap consistent with the evidence is a sign-changing state in the A_{1g} irreducible representation (irrep) of the point group. Although nodes are not required by the symmetry of the order parameter, "accidental" nodes depending on the microscopic details of the system are possible, as is the case in some pnictide compounds[39]. To realize this, we propose a gap function with both isotropic and anisotropic components,

$$\Delta(\hat{\boldsymbol{k}}) = \Delta_0 C_r[r + (1-|r|)(\hat{k}_x^4 + \hat{k}_y^4 + \hat{k}_z^4)] \quad (1)$$

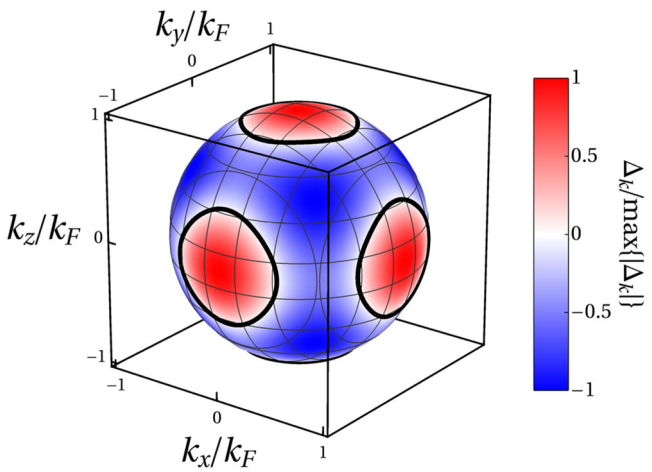

Fig. 2 | Superconducting gap in $Rh_{17}S_{15}$. Suggested superconducting gap in $Rh_{17}S_{15}$ with $r = -0.4$ in Eq.(1). The solid black lines represent the nodes. The color scale bar indicates the relative gap magnitude.

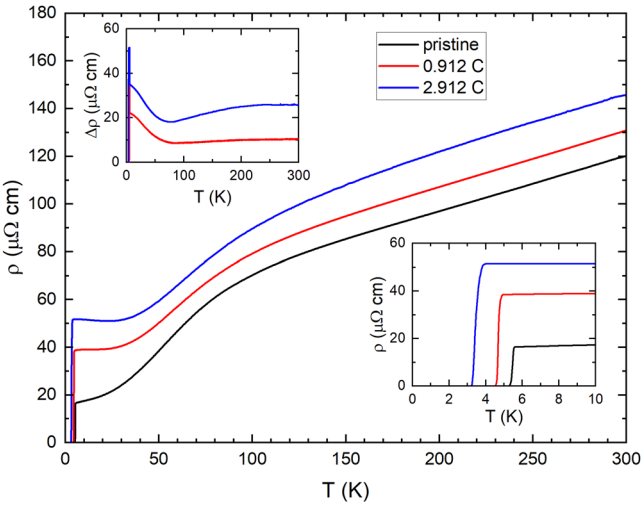

Fig. 3 | Effect of electron irradiation on electrical resistivity of $Rh_{17}S_{15}$. Temperature-dependent resistivity of single crystalline sample, S-2, before irradiation in the pristine state (black line) and after 0.912 C cm^{-2} (red line) and 2.912 C cm^{-2} (blue line) electron irradiation. The upper inset shows the temperature-dependent difference between irradiated and pristine curves, revealing a clear Matthiessen's rule violation below 100 K. The lower inset zooms in on the superconducting transition region.

where $-1 \le r \le 1$ tunes the relative strength and sign of the isotropic and anisotropic gap components, and C_r is a normalization constant chosen so that the Fermi-surface average of $|\Delta(\hat{\boldsymbol{k}})|^2$ is independent of r (see Supplementary Note 3 for details)). This gap structure is visualized in Fig. 2 for $r = -0.4$. For a spherical Fermi surface, Eq. (1) includes the lowest power of k that gives an anisotropic A_{1g} gap, and has line nodes for $-0.5 < r < -0.25$. As shown in Fig. 1b, the calculated superfluid density[22] is in quantitative agreement with the experiment for $-0.45 \le r \le -0.4$, which corresponds to circular line nodes centered about the crystal axes (see Supplementary Note 3 for details).

Other nodal states are strongly constrained by the cubic crystal symmetry. For example, although the three-dimensional d-wave state $\Delta(\hat{\boldsymbol{k}}) = \sqrt{15/4}\Delta_0(\hat{k}_x^2 - \hat{k}_y^2)$ in the E_g irrep is consistent with the penetration depth data, it reduces the symmetry from cubic to tetragonal[40]. Such a nematic superconducting state is highly exotic, having so far only been observed in the Bi_2Se_3 family[41]. The nematicity is reflected in the superfluid density, which only fits the data for an in-plane field. In general, a nematic superconductor possesses multiple nematic domains with different orientations of the order parameter. We expect this to lead to a measured superfluid density in between the extreme limits of the in-plane and out-of-plane responses. However, our data is only consistent with a monodomain sample. Although we cannot fully exclude a nematic state in the E_g irrep, the isotropic superfluid density of the A_{1g} state makes the latter a more conservative scenario. Pairing states in other nontrivial irreps are also unlikely since they imply nematic or high-angular-momentum pairing states.

Effect of disorder on the superconducting transition temperature

An independent test for a sign-changing superconducting gap function was made by studying the effect of nonmagnetic disorder on T_c. This disorder was introduced in a controlled manner by low-temperature electron irradiation, which is a known method to introduce a metastable population of vacancies[42,43], see Supplementary Note 4 for details. Figure 3 shows the temperature-dependent resistivity of single crystalline sample S-2 of $Rh_{17}S_{15}$ before irradiation in the pristine state (black line) and after electron irradiations with two doses of 0.912 C/cm^2 (red line) and 2.912 C/cm^2 (blue line), respectively. The upper inset shows the temperature-dependent difference where pristine-state data were subtracted from the data after the irradiation. A clear violation of the Matthiessen rule is observed below about

100 K. The lower inset in Fig. 3 zooms in on the superconducting transition region. A clear suppression of T_c is evident, with a reduction of 26% and 40% after irradiation with 0.912 C/cm^2 and 2.912 C/cm^2, respectively.

We have no evidence that the irradiation of $Rh_{17}S_{15}$ introduces magnetic impurities, and therefore, here we deal only with the effect of nonmagnetic impurities. Their effect in a superconductor with an anisotropic gap is to smear out the anisotropy, with the order parameter reaching its average value in the dirty limit. This is accompanied by a suppression of the critical temperature; at low disorder strength, the suppression is approximately linear[44–46]

$$t_c = \frac{T_c}{T_{c0}} \approx 1 - \left(1 - \langle\hat{\Delta}_{\mathbf{k}}\rangle^2\right)\frac{\pi^2}{4}\Gamma \qquad (2)$$

where $\langle\hat{\Delta}_{\mathbf{k}}\rangle$ is the Fermi surface average of the normalized form factor of the pairing potential, and $\Gamma = \hbar/(2\pi k_B T_{c0}\tau)$ is the dimensionless scattering rate, T_{c0} is the transition temperature in the clean limit, and τ is the scattering time in the normal state. In the two extreme limits of a uniform gap ($\langle\hat{\Delta}_{\mathbf{k}}\rangle = 1$) there is no suppression of T_c, whereas the suppression is maximal for a sign-changing d-wave gap ($\langle\hat{\Delta}_{\mathbf{k}}\rangle = 0$); the sign-changing A_{1g} state Eq. (1) lies between these two limits. Thus, the slope $dt_c/d\Gamma$ gives an independent check on the gap structure inferred from the superfluid density.

In the Drude model, the resistivity is $\rho = m/(ne^2\tau)$, and in London electrodynamics, the penetration depth is $\lambda^2 = m/(\mu_0 ne^2)$, where $\mu_0 = 4\pi \times 10^{-7}$ H/m is the vacuum magnetic permeability. Therefore, we can express the dimensionless scattering rate via measurable parameters,

$$\Gamma = \frac{\hbar}{2\pi k_B T_{c0}\tau} = \frac{\hbar\rho_0}{2\pi k_B \mu_0 T_{c0}\lambda^2(0)} \qquad (3)$$

In our case $T_{c0} = 5.4$ K and $\lambda(0) = 550$ nm. As can be seen in the lower insert, the $\rho(T)$ curves saturate approaching T_c from above, and so the values of the resistivity at T_c are good approximations for ρ_0.

Unfortunately, the experimental $\rho(T)$ in $Rh_{17}S_{15}$ is qualitatively different from the conventional Bloch–Gruneisen theory[47]. Moreover, around 100 K, the Hall effect changes sign, and a notable non-linearity of its field dependence emerges[11,32]. The analysis of the field-dependent resistivity and Hall effect finds at least two groups of carriers with notable differences in properties conducting in parallel. The low-temperature transport is dominated by high mobility carriers with mobilities up to 600 cm^2/(V s), while carriers with normal metallic mobilities of order 1 cm^2/(V s) are responsible for resistivity at high temperatures[32]. The difference in mobilities naturally explains a significantly greater increase in resistivity at low temperatures after irradiation[48,49]. This extreme difference in the properties of the carriers makes it harder to determine a single effective scattering rate from resistivity change[44]. The origin of the high-mobility carriers is unclear. Although the shoulder-like feature in Fig. 3 is rather smooth and broad, somewhat sharper features similar to this are observed in three-dimensional materials undergoing charge density wave instability[50] (See Supplementary Note 5 for details). High mobility carriers there may arise from small pockets forming upon Fermi surface reconstruction. To eliminate this possibility, we measured X-ray diffraction and did not find any additional peaks down to 5 K (see Supplementary Note 6 for details).

Despite the significant temperature dependence in the resistivity change by electron irradiation, it is still possible to use Eq. (3) to estimate the scattering rate. Specifically, we use two limiting values, one estimated at T_c where high mobility carriers dominate and another at room temperature determined by normal carriers, giving the results in Fig. 4 by open and filled symbols, respectively. The corresponding rates of suppression $dt_c/d\Gamma$ are approximately −2 and −4 in these two cases. The straight lines in Fig. 4 show the expected T_c suppression for the order parameter of Eq.(1). The isotropic s-wave case corresponds to $r = -1$ (black solid line), while the dotted line is for $r = -0.45$ and the dashed line is for $r = -0.4$. The latter values are most consistent with the fit to the superfluid density. The

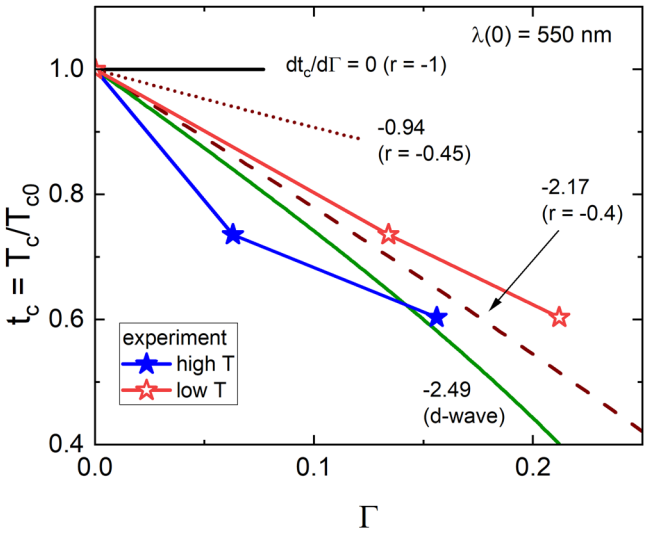

Fig. 4 | Suppression of T_c/T_{c0} vs. Γ for various r in $Rh_{17}S_{15}$ compared to typical gap symmetries. See text for the definitions of Γ and r. The closed and open star symbols represent the calculated Γ with $\Delta\rho$ (see Fig. 2) at room temperature and low temperature, respectively.

agreement with the experimental data is closer for $r = -0.4$, which is also close to a d-wave order parameter shown in Fig. 4 by a green solid line. The strong suppression of the transition temperature, therefore, supports the existence of a sign-changing superconducting gap function in $Rh_{17}S_{15}$ and is consistent with the fits to the superfluid density.

Effect of disorder on the upper critical field

The high upper critical field of $Rh_{17}S_{15}$, $H_{c2}(0) \approx 20$ T[7], suggests that the carriers involved in superconducting pairing should be rather heavy, since $H_{c2} \sim v_F^{-2}$, where v_F is Fermi velocity[19,51]. On the contrary, the London penetration depth and resistivity are dominated by light carriers. To access the properties and response to the disorder of the heavier carriers in the condensate, we measured the upper critical field of the pristine and irradiated samples, with the results shown in Fig. 5a. In the pristine state, $H_{c2}(T)$ as determined from the onset of resistivity in our measurements (complete symbols) is perfectly consistent with the definition of entropy balance from the specific heat measurements shown by open triangles[35]. After irradiation with the doses of 0.912 C (red squares) and 2.912 C (blue triangles), the $H_{c2}(T)$ curves are shifted to lower temperatures with a slight decrease of the slope at T_c. See Supplementary Note 7 for details.

In our analysis of the upper critical field H_{c2}, we utilize the fact that the behavior of an isotropic s-wave superconductor with magnetic impurities is practically the same as the behavior of a d-wave superconductor with nonmagnetic impurities[52,53]. This reflects the sensitivity of anisotropic pairing to potential disorder and considerably simplifies the calculation of the upper critical field[19,54]. Since the suppression of the T_c reveals a gap with anisotropy comparable to a pure d-wave state, this should be a good approximation for $Rh_{17}S_{15}$. We therefore consider an s-wave pairing state with distinct scattering rates for the nonmagnetic and magnetic disorder, Γ_0 and Γ_m, respectively. The latter is usually associated with scattering on point-like magnetic impurities where the spins of a scattered electron and the impurity flip. In a singlet superconductor, where the spins in a Cooper pair are antiparallel, the reversal of one of them breaks the pair. Nonmagnetic scattering between regions of the Fermi surface with opposite gap signs in $Rh_{17}S_{15}$ has a comparably deleterious effect on the superconductivity, justifying the magnetic scattering rate in our theory.

The theoretical curves, panels b, c, and d in Fig. 5, illustrate the effects of different types of disorder on H_{c2} as calculated from the Eilenberger theory[19,54]. The theory is parameterized by dimensionless non-pair-breaking and pair-breaking scattering rates Γ_0 and Γ_m, respectively; we note that these are distinct from the scattering rate introduced in Eq. (3). Reviewing the

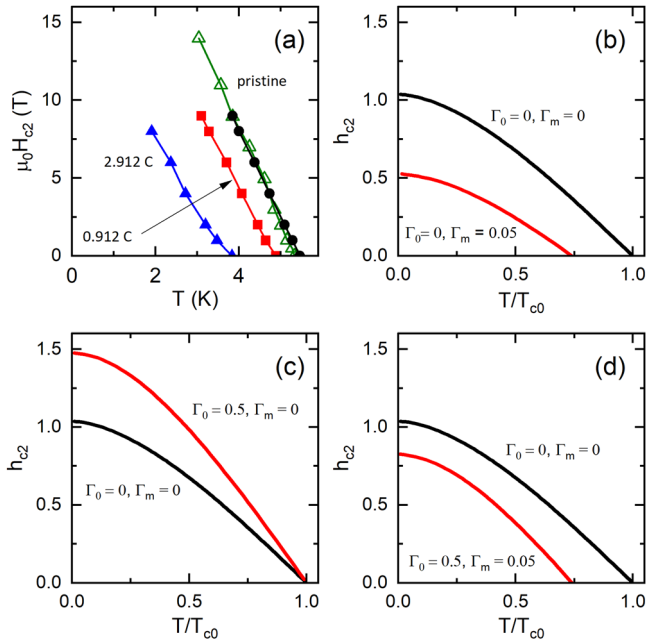

Fig. 5 | Temperature-dependent upper critical field in $Rh_{17}S_{15}$. a Temperature-dependent upper critical field in a pristine single crystal of $Rh_{17}S_{15}$ (black curve) and electron-irradiated samples with doses of 0.912 C cm^{-2} (red squares) and 2.912 C cm^{-2} (blue triangles). The onset of resistivity was used as a criterion. The complete dataset is shown in Supplementary Fig. 6. Measurements were taken in the magnetic fields parallel to [100] crystallographic direction. The green open triangles show H_{c2} determined from heat capacity measurements in polycrystalline samples[35]. **b**–**d** The evolution of $H_{c2}(T)$ with the pairbreaking (Γ_m) and potential (Γ_0) scattering[19,54]. The corresponding scattering rates are indicated in each panel.

results shows that non-pairbreaking scattering always increases $H_{c2}(0)$ and its slope at T_c, whereas pair-breaking scattering, which is expected in nodal superconductors with non-magnetic disorder, suppresses both $H_{c2}(0)$ and its slope at T_c. This is consistent with the trend observed in our experiment and provides the third independent evidence that $Rh_{17}S_{15}$ is a nodal unconventional superconductor.

Conclusions

We have discovered a rare occurrence of nodal superconductivity in the cubic 4*d*-electron compound $Rh_{17}S_{15}$. Our conclusions are based on the linear temperature variation of the London penetration depth and the suppression of the transition temperature and the upper critical field by non-magnetic disorder introduced by electron irradiation. The analysis of the superfluid density and the T_c suppression rate is consistent with an extended *s*-wave superconducting state with accidental line nodes preserving cubic symmetry. Our results suggest that pure $Rh_{17}S_{15}$ is the first known unconventional superconductor among materials that also exist in mineral form. However, a large amount of impurities, such as iron, nickel, platinum, and copper, known to be present in natural minerals at a level of a few percent[13], make it highly unlikely that they will exhibit superconductivity. Nature knows how to hide its secrets.

Methods

Single crystal growth

To investigate the superconducting state in $Rh_{17}S_{15}$, we synthesized single crystalline samples out of the Rh-S eutectic region by using a high-temperature flux growth technique. In Ref. [5], it has been shown that the high-temperature solution growth technique can be used to grow binary and ternary transition metal-based compounds out of S-based solutions. In refs. [55,56], high-temperature solution growth was expanded to Rh–S–X ternaries. As part of that effort, we re-determined the Rh-rich eutectic composition to be close to $Rh_{60}S_{40}$. As a result, we were able to create a slightly more S-rich melt, $Rh_{58}S_{42}$, by combining elemental Rh powder (99.9+ purity) and elemental S in a fritted Canfield Crucible set[57], sealing in a silica ampoule, slowly heating (over 12 h) to 1150 °C and then slowly cooling from 1150 to 920 °C over 50 h and decanting[58]. Millimeter-sized single crystals of $Rh_{17}S_{15}$ grew readily (see inset to Fig. 1a).

Electron irradiation

The low-temperature 2.5 MeV electron irradiation was performed at the SIRIUS Pelletron facility of the Laboratoire des Solides Irradiés (LSI) at the Ecole Polytechnique in Palaiseau, France. The acquired irradiation dose is conveniently expressed in C/cm^2 and measured directly as a total charge accumulated behind the sample by a Faraday cage. Therefore, 1 C/cm^2 ≈ 6.24 × 10^{18} electrons/cm^2. The irradiation was carried out with the sample immersed in liquid hydrogen at about 20 K. See Supplementary Note 4 for details.

Electrical transport

Four probe electrical resistivity measurements were performed in *Quantum Design* PPMS on three samples S-2, S-3, and S-4. Contacts to the samples were soldered with tin[59] and had resistance in mΩ range (See Supplementary Note 8 for details). Resistivity measurements were made on the same samples without contact remounting before and after irradiation to exclude the uncertainty of geometric factor determination.

Tunnel diode resonator

The London penetration depth was measured by using a TDR technique[60]. The shift of the resonant frequency (in cgs units), $\Delta f(T) = -G4\pi\chi(T)$, where $\chi(T)$ is the differential magnetic susceptibility, $G = f_0 V_s / 2V_c(1-N)$ is a constant, N is the demagnetization factor, V_s is the sample volume and V_c is the coil volume. The constant G was determined from the full frequency change by physically pulling the sample out of the coil. With the characteristic sample size, R, $4\pi\chi = (\lambda/R)\tanh(R/\lambda) - 1$, from which $\Delta\lambda$ can be obtained[22,60], see Supplementary Note 1 for details.

Data availability

The authors declare that the data supporting the findings of this study are available within the paper and its supplementary information. Data sets generated during the current study are available from the corresponding author upon reasonable request.

Received: 27 June 2023; Accepted: 5 February 2024;
Published online: 17 February 2024

References

1. Wampler, J., Thiemens, M., Cheng, S., Zhu, Y. & Schuller, I. K. Superconductivity found in meteorites. *Proc. Natl. Acad. Sci. USA* **117**, 7645 (2020).
2. Di Benedetto, F. et al. First evidence of natural superconductivity: covellite. *Eur. J. Mineral.* **18**, 283 (2006).
3. Meissner, W. Messungen mit Hilfe von flüssigem Helium. V. Supraleitfähigkeit von Kupfersulfid. *Z. Phys.* **58**, 570 (1929).
4. Sakamoto, T., Wakeshima, M. & Hinatsu, Y. Superconductivity in ternary chalcogenides $Bi_2Ni_3X_2$ (X = S, Se). *J. Phys. Condens. Matter* **18**, 4417 (2006).
5. Lin, X., Bud'ko, S. L. & Canfield, P. C. Development of viable solutions for the synthesis of sulfur bearing single crystals. *Philos. Mag.* **92**, 2436 (2012).
6. Matthias, B. T., Corenzwit, E. & Miller, C. E. Superconducting compounds. *Phys. Rev.* **93**, 1415 (1954).
7. Naren, H. R., Thamizhavel, A., Auluck, S., Prasad, R. & Ramakrishnan, S. Normal state and superconducting properties of $Rh_{17}S_{15}$ and $Pd_{17}Se_{15}$. *Supercond. Sci. Technol.* **24**, 105015 (2011).
8. Juza, R., Hiilamann, O., Meisel K. & Biltz, W. *Z.*Beiträge zur systematischen Verwandtschaftslehre. Über Die Sulfide des Rhodiums Anorg. *Allgem. Chem*. **225**, 369 (1935).

9. Geller, S. The crystal structure of the superconductor $Rh_{17}S_{15}$. *Acta Cryst.* **15**, 1198 (1962).
10. Britvin, S., Rudashevsky, N., Bogdanova, A. & Shcherbachev, D. Miassite Rh17S15, a new mineral from a placier of Miass River. *Urals. Zap. Vseross. Mineral. Obshch.* **130**, 41 (2001).
11. Naren, H. R., Thamizhavel, A., Nigam, A. K. & Ramakrishnan, S. Strongly Correlated Superconductivity in $Rh_{17}S_{15}$. *Phys. Rev. Lett.* **100**, 026404 (2008).
12. Belkin, H. E. & Grosz, A. E. Platinum and gold placer from Tugidak Island, Alaska: Platinum-group minerals and their inclusions, gold, and chromite mineralogy. *Can. Mineral.* **59**, 667 (2021).
13. website, https://www.handbookofmineralogy.org/pdfs/Miassite.pdf.
14. Settai, R. et al. Superconducting properties in $Rh_{17}S_{15}$ under magnetic field and pressure. *J. Phys. Chem. Solids* **71**, 700 (2010).
15. Casaca, A., Lopes, E. B., Gonçalves, A. P. & Almeida, M. Electrical transport properties of CuS single crystals *J. Phys. Condens. Matter* **24**, 015701 (2011).
16. Koyama, T. et al. Electron Correlations in Superconductor $Rh_{17}S_{15}$ studied by ^{103}Rh NMR and Specific Heat Measurements. *J. Phys. Soc. Jpn.* **79**, 114723 (2010).
17. White, B., Thompson, J. & Maple, M. Unconventional superconductivity in heavy-fermion compounds. *Physica C* **514**, 246 (2015).
18. Fukui, M. et al. Photoemission Study of $Rh_{17}S_{15}$ Superconductor. *J. Phys. Soc. Jpn.* **80**, SA111 (2011).
19. Kogan, V. G. & Prozorov, R. Orbital upper critical field and its anisotropy of clean one- and two-band superconductors. *Rep. Prog. Phys.* **75**, 114502 (2012).
20. Benfatto, L., Toschi, A., Caprara, S. & Castellani, C. Coherence length in superconductors from weak to strong coupling. *Phys. Rev. B* **66**, 054515 (2002).
21. Hardy, W. N., Bonn, D. A., Morgan, D. C., Liang, R. & Zhang, K. Precision measurements of the temperature dependence of λ in $YBa_2Cu_3O_{6.95}$: Strong evidence for nodes in the gap function. *Phys. Rev. Lett.* **70**, 3999 (1993).
22. Prozorov, R. & Giannetta, R. W. Magnetic penetration depth in unconventional superconductors. *Supercond. Sci. Technol.* **19**, R41 (2006).
23. Tsuei, C. C. & Kirtley, J. R. Pairing symmetry in cuprate superconductors. *Rev. Mod. Phys.* **72**, 969 (2000).
24. Fukazawa, H. et al. Possible multiple gap superconductivity with line nodes in heavily hole-doped superconductor KFe_2As_2 studied by ^{75}As nuclear quadrupole resonance and specific heat. *J. Phys. Soc. Jpn.* **78**, 083712 (2009).
25. Dong, J. K. et al. Quantum criticality and nodal superconductivity in the FeAs-based superconductor KFe_2As_2. *Phys. Rev. Lett.* **104**, 087005 (2010).
26. Reid, J.-P. et al. Nodes in the gap structure of the iron arsenide superconductor $Ba(Fe_{1-x}Co_x)_2As_2$ from *c*-axis heat transport measurements. *Phys. Rev. B* **82**, 064501 (2010).
27. Mizukami, Y. et al. Disorder-induced topological change of the superconducting gap structure in iron pnictides. *Nat. Commun.* **5**, 5657 (2014).
28. Wosnitza, J. Quasi-two-dimensional organic superconductors. *J. Low Temp. Phys.* **146**, 641 (2007).
29. Van Degrift, C. T. Tunnel diode oscillator for 0.001 ppm measurements at low temperatures. *Rev. Sci. Instrum.* **46**, 599 (1975).
30. Kim, H., Tanatar, M. A. & Prozorov, R. Tunnel diode resonator for precision magnetic susceptibility measurements in a mK temperature range and large dc magnetic fields. *Rev. Sci. Instrum.* **89**, 094704 (2018).
31. De Gennes, P. *Superconductivity Of Metals And Alloys* (Boca Raton, CRC Press, 2018).
32. Daou, R., Berthebaud, D. & Maignan, A. Suppression of superconductivity and resistivity anomaly in $Rh_{17}S_{15}$ by cobalt substitution. *J. Phys. Condens. Matter* **29**, 075604 (2016).
33. Naren, H. R., Arumugam, T. & Ramakrishan, S. Superconductivity in $Rh_{17}S_{15}$ and $Pd_{17}Se_{15}$: a comparative study. *J. Phys. Condens. Matter* **273**, 012074 (2011).
34. Kim, H., Kogan, V. G., Cho, K., Tanatar, M. A. & Prozorov, R. Rutgers relation for the analysis of superfluid density in superconductors. *Phys. Rev. B* **87**, 214518 (2013).
35. Uhlarz, M. et al. Superconducting phase diagram of $Rh_{17}S_{15}$. *J. Low Temp. Phys.* **159**, 176 (2010).
36. Diéguez, O. & Marzari, N. First-principles characterization of the structure and electronic structure of α-S and Rh-S chalcogenides. *Phys. Rev. B* **80**, 214115 (2009).
37. Sung, N. H., Jo, Y. J. & Cho, B. K. Hall sign reversal and electrical transport properties of single crystalline $SrPd_2Ge_2$. *J. Appl. Phys.* **109**, 07E109 (2011).
38. Kim, H., Sung, N. H., Cho, B. K., Tanatar, M. A. & Prozorov, R. Magnetic penetration depth in single crystals of $SrPd_2Ge_2$ superconductor. *Phys. Rev. B* **87**, 94515 (2013).
39. Yamashita, M. et al. Nodal gap structure of superconducting $BaFe_2(As_{1-x}P_x)_2$ from angle-resolved thermal conductivity in a magnetic field. *Phys. Rev. B* **84**, 060507 (2011).
40. Sigrist, M. & Ueda, K. Phenomenological theory of unconventional superconductivity. *Rev. Mod. Phys.* **63**, 239 (1991).
41. Matano, K., Kriener, M., Segawa, K., Ando, Y. & Zheng, G.-q Spin-rotation symmetry breaking in the superconducting state of $Cu_xBi_2Se_3$. *Nat. Phys.* **12**, 852 (2016).
42. Damask A. & Dienes, G. *Point Defects in Metals* (Gordon and Breach, 1963).
43. Thompson, M. *Defects and Radiation Damage in Metals*, Cambridge Monographs on Physics (Cambridge University Press, 1969).
44. Prozorov, R. et al. Effect of electron irradiation on superconductivity in single crystals of $Ba(Fe_{1-x}Ru_x)_2As_2$ ($x = 0.24$). *Phys. Rev. X* **4**, 041032 (2014).
45. Kogan, V. G. & Prozorov, R. Interband coupling and nonmagnetic interband scattering in $\pm s$ superconductors. *Phys. Rev. B* **93**, 224515 (2016).
46. Timmons, E. I. et al. Electron irradiation effects on superconductivity in $PdTe_2$: an application of a generalized Anderson theorem. *Phys. Rev. Res.* **2**, 023140 (2020).
47. Allen, P. B. Metals with small electron mean-free path: saturation versus escalation of resistivity. *Phys. B: Condens. Matter.* **318**, 24 (2002).
48. Bass, J. Deviations from Matthiessen's Rule. *Adv. Phys.* **21**, 431 (1972).
49. Blomberg, E. C. et al. Multi-band effects in in-plane resistivity anisotropy of strain-detwinned disordered $Ba(Fe_{1-x}Ru_x)_2As_2$. *J. Phys. Condens. Matter* **30**, 315601 (2018).
50. Naito, M. & Tanaka, S. Electrical transport properties in 2H-NbS_2, -$NbSe_2$, -TaS_2 and -$TaSe_2$. *J. Phys. Soc. Jpn.* **51**, 219 (1982).
51. Helfand, E. & Werthamer, N. R. Temperature and purity dependence of the superconducting critical field, H_{c2}. II. *Phys. Rev.* **147**, 288 (1966).
52. Abrikosov, A. A. & Gor'kov, L. P. Contribution to the theory of superconducting alloys with paramagnetic impurities. *Zh. Eksp. Teor. Fiz.* **39**, 1781 (1960) [Sov. Phys. JETP 12, 1243 (1961)].
53. Openov, L. A. Effect of nonmagnetic and magnetic impurities on the specific heat jump in anisotropic superconductors. *Phys. Rev. B* **69**, 224516 (2004).
54. Kogan, V. G. & Prozorov, R. Disorder-dependent slopes of the upper critical field in nodal and nodeless superconductors. *Phys. Rev. B* **108**, 064502 (2023).
55. Kaluarachchi, U. S. et al. Superconductivity versus structural phase transition in the closely related $Bi_2Rh_{3.5}S_2$ and $Bi_2Rh_3S_2$. *Phys. Rev. B* **91**, 174513 (2015).

56. Kaluarachchi, U. S. et al. Superconducting properties of $Rh_9In_4S_4$ single crystals. *Phys. Rev. B* **93**, 094524 (2016).
57. Canfield, P. C., Kong, T., Kaluarachchi, U. S. & Jo, N. H. Use of frit-disc crucibles for routine and exploratory solution growth of single crystalline samples. *Philos. Mag.* **96**, 84 (2016).
58. Canfield, P. C. New materials physics. *Rep. Prog. Phys.* **83**, 016501 (2019).
59. Tanatar, M. A., Ni, N., Bud'ko, S. L., Canfield, P. C. & Prozorov, R. Field-dependent transport critical current in single crystals of $Ba(Fe_{1-x}TM)_2As_2$. *Supercond. Sci. Technol.* **23**, 054002 (2010).
60. Prozorov, R. & Kogan, V. G. London penetration depth in iron-based superconductors. *Rep. Prog. Phys.* **74**, 124505 (2011).

Acknowledgements

PCC acknowledges the Encyclopedia of Minerals (Second Edition), by W. L. Roberts, T. J. Campbell, and G. R. Rapp, as a continued source of inspiration. PCC and SLB acknowledge Xiao Lin for having helped to initiate studies of $Rh_{17}S_{15}$. We are grateful for the useful discussions with V. Kogan, P. Hirschfeld, R. Daou, J. Paglione, and D. Agterberg. We thank S. Ghimire and K. Joshi for their help with the penetration depth measurements. Work in Ames was supported by the U.S. Department of Energy (DOE), Office of Science, Basic Energy Sciences, Materials Science and Engineering Division. Ames Laboratory is operated for the U.S. DOE by Iowa State University under contract DE-AC02-07CH11358. The authors acknowledge support from the EMIR&A French network (FR CNRS 3618) on the platform SIRIUS. This research used resources of the Advanced Photon Source, a U.S. Department of Energy (DOE) Office of Science User Facility, operated for the DOE Office of Science by Argonne National Laboratory under Contract No. DE-AC02-06CH11357. PMRB was supported by the Marsden Fund Council from Government funding, managed by Royal Society Te Apārangi, Contract No. UOO2222.

Author contributions

R.P. and P.C.C. conceived the project. U.S.K. and P.C.C. grew single crystal samples used in this study. M.A.T. prepared the samples and performed transport measurements. H.K., S.T., and K.C. conducted the London penetration depth measurements and carried out the analysis. M.A.T., R.P., M.K., and R.G. conducted electron irradiation experiments. A.S., J.M.W, and M.J.K conducted X-ray diffraction experiments. R.P. and P.M.R.B. performed theoretical calculations. H.K., M.A.T., R.P., P.M.R.B., S.L.B., and P.C.C. wrote the paper with input from all authors.

Competing interests

The authors declare no competing interests.

Additional information

Supplementary information The online version contains supplementary material available at https://doi.org/10.1038/s43246-024-00456-w.

Correspondence and requests for materials should be addressed to Ruslan Prozorov.

Peer review information *Communications Materials* thanks the anonymous reviewers for their contribution to the peer review of this work. Primary Handling Editors: Nicola Poccia and Aldo Isidori.